Proceedings of the ASME 2015 9th International Conference on Energy Sustainability
ES2015
June 28-July 2, 2015, San Diego, California

ES2015-49481

ASSESSMENT OF PHOTOVOLTAIC SURFACE TEXTURING ON TRANSMITTANCE EFFECTS AND GLINT/GLARE IMPACTS

Julius Yellowhair and Clifford K. Ho

Sandia National Laboratories, Albuquerque, New Mexico, 87185-1127, USA, (505) 844-2384, jeyello@sandia.gov

ABSTRACT

Standard glass and polymer covers on photovoltaic modules can partially reflect the sunlight causing glint and glare. Glint and glare from large photovoltaic installations can be significant and have the potential to create hazards for motorists, air-traffic controllers and pilots flying near installations. In this work, the reflectance, surface roughness and reflected solar beam spread were measured from various photovoltaic modules acquired from seven different manufacturers. The surface texturing of the PV modules varied from smooth to roughly textured. Correlations between the measured surface texturing (roughness parameters) and beam spread (subtended angle) were determined. These correlations were then used to assess surface texturing effects on transmittance and ocular impacts of glare from photovoltaic module covers. The results can be used to drive the designs for photovoltaic surface texturing to improve transmittance and minimize glint/glare.

NOMENCLATURE

E – Irradiance (W/m^2)
DNI – Direct normal irradiance (1,000 W/m^2 is typical)
θ_i – Source angle of incidence (e.g. from the sun) (deg)
ρ – Reflectance of the PV module
S_a – 2D average surface roughness (μm)
S_q – 2D RMS surface roughness (μm RMS)
S_z – 2D surface roughness peak-to-valley surface height (μm)
Λ – Surface spatial period (mm)
β, ω – Reflected beam spread or source subtended angle (mrad)
d_p – Eye pupil diameter (~0.2 cm)
τ – Eye transmittance (~0.5)
f – Eye focal length (~1.7 cm)

1. INTRODUCTION

As the cost of photovoltaic (PV) modules continues to drop, large-scale deployments of PV are on the rise [1]. A typical construction of a PV module includes a robust panel structure enclosing the solar cells and wiring, and a transparent front cover, typically glass or polymer, which protects and transmits sunlight to the solar cells. The nature of the glass/polymer cover exposed to air will partially reflect some of the incident sunlight, by Fresnel reflections, creating glint and glare. PV modules on fixed tilt racks will produce glint/glare in certain regions around the PV field depending on the sun position and tilt angles of the PV modules. The magnitude of the reflectance from the glass/polymer cover depends on the reflectance (ρ) as a function of incidence angle (θ_i), the smoothness (or roughness) of the surface, and the sun irradiance and position. These parameters will dictate the glint/glare intensity. Recently, there have been reports on glint/glare hazards near PV fields [2]-[4]. Depending on the glare intensity, a momentary glare exposure can cause temporary after-image or disability glare, which can be a hazard for pilots and drivers.

Smooth, bare glass (e.g., car windshield) is known to reflect sunlight specularly. Bare glass reflects about 4% of the incident light at normal incidence angle. However, the reflectance increases rapidly at higher incidence angles [5]. In addition to the magnitude of the reflectance from the surface of PV glass modules, the amount of glare from the glass surfaces can be affected by the surface texturing. Surface texturing, in general, causes the reflected beam to spread out due to additional scattering from diffuse reflections [6]. A more diffuse reflection can reduce the glare intensity for a constant source irradiance. In this study, the surface roughness of the PV glass covers was measured and a correlation between surface texturing (quantified as the surface roughness and the

periodicity of the texture) and glare (angular spread of the reflected beam) was determined.

The first section of this paper describes methods for measuring parameters (e.g., surface roughness and solar reflected beam spread) and discusses ocular hazards from glint/glare. The results are provided in the next section. Discussion of the approach and results is then provided. Finally, concluding comments and future work plans are provided. Some representative measured surface data are provided in the Appendix.

2. APPROACH

2.1. Surface Roughness Measurements

The surface roughness of the PV module samples were measured with a Taylor-Hobson Talysurf optical profilometer. A total of 26 PV module samples, from seven different companies, with varying surface types were measured. The PV modules were too large to fit under the optical profilometer. Therefore, small areas (~40-50 mm diameter) of the PV module surfaces were replicated, and then the surface replicas were measured with the optical profilometer.

A two-part rubber, putty compound (Flexbar ReproRubber) was used to replicate the PV module surfaces. The PV modules were cleaned using water, mild soap, and lint-free cloth. Equal parts of the base and catalyst putty were mixed by kneading. The mixture was spread over the surface to be replicated and light pressure was applied. The rubber compound hardened after about five minutes, after which it was carefully removed from the surface.

The replicated samples (replicas) were measured with the optical profilometer for surface roughness. Data was collected using the native Talysurf software. The replicas had low reflectance in addition to the relatively rough surfaces. Therefore, the "peak intensity correlation" option was used to measure surface heights over 1.7 mm × 1.7 mm areas, instead of the standard "phase shifting" approach, which requires smooth surfaces and reflectivities of >40%. To increase the measurement area, four measurements (2 × 2 array) were acquired with some overlap of the measurements. The data stitching algorithm in Talysurf was then used to combine the four measurements to synthesize a larger measurement area (about 3 mm × 3 mm). Further data analysis was performed using Mountain Digital Surf and Matlab® software packages. The Digital Surf software was used to remove tilt and low-order form errors from the data and then calculate the two-dimensional (2D) surface roughness parameters (S_a, S_q, S_z) [7]. Matlab was used to remove higher order form errors and perform a Fourier analysis to determine surface spatial period variations on the samples; the spatial period (mm) is the inverse of the spatial frequency (1/mm). Figure 1 shows a flow diagram of the overall measurement process starting with the PV preparation for the surface replications.

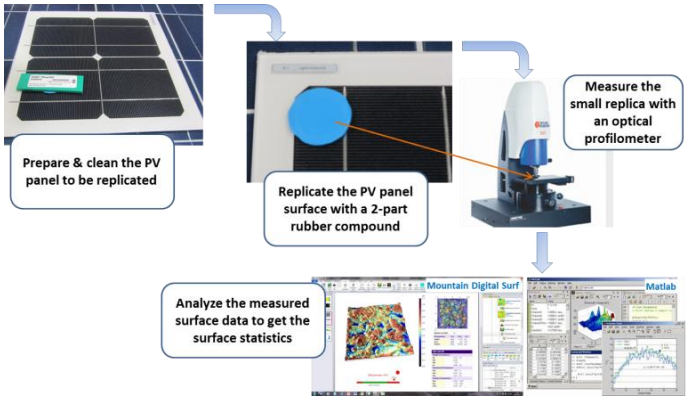

Figure 1. Flow diagram for quantifying the PV modules surface texturing. 1) PV module surfaces were cleaned and replicated, 2) replicas were measured with an optical profilometer, and 3) the surface data were analyzed.

One of the developmental PV samples, which was a single-cell module, was small enough to fit on the optical profilometer sample holder. This sample was used to verify the accuracy of our surface replication process; the actual PV module surface was measured directly and compared to the measurements on the replica to get an indication of the replication accuracy. The RMS surface roughness agreed to within 7% between the replica and the actual surface (after two measurements on both). The replicas generally had higher RMS surface roughness values. This could be due to form errors that remained in the surface measurements. Although the rubber-like replicas were thick (3-4 mm), they could bend and flex slightly. In addition, the replicas surface data were more "grainy" as seen in Figure 8 in the Appendix.

2.2. Solar Reflected Beam Spread Measurements

The beam spread (glare) from the PV modules was measured outdoors by observing the sun (during clear sky days) in reflection through the PV modules. Figure 2 shows examples of the reflected sun image on different PV module samples. Twenty-one of the 26 PV modules were measured for glare. Using a digital camera (Nikon D90), raw (or unscaled) photos of the reflected sunlight were collected. By knowing the distance between the camera and PV module, the angular beam spread after reflection (i.e., angle subtended by the visible glare spot due to specular reflection) was calculated through image processing of the photos in Matlab.

Figure 2. Examples of solar glare and beam spread resulting from different PV glass samples, with varying surface texture, captured with a digital camera (Permission from [3]). Left: smooth glass. Middle: Lightly textured glass with anti-reflective coating. Right: Deeply textured glass. Samples courtesy of Canadian Solar, Inc.

2.3. Ocular Hazards Chart

Impacts of glint and glare on eyesight can include discomfort, disability, veiling effects, after-image and retinal burn [2]. Prolonged exposure to "discomfort glare" may lead to headaches and other physiological impacts, whereas "disability glare" immediately reduces visual performance. Disability glare can include after-image effects, flash blindness and veiling, such as that caused by solar glare on a windshield that might mask pedestrians, vehicles, or aircraft. Retinal burn can occur with exposure to lasers or concentrated sunlight.

Ho, *et al*. [4] developed irradiance models and summarized the potential impacts to eyesight as a function of retinal irradiance (the solar flux entering the eye and reaching the retina) and subtended source angle (size of glare source divided by distance). Figure 3 shows the resulting "Ocular Hazard Plot" with three regions: (1) potential for permanent eye damage (retinal burn), (2) potential for temporary after-image, and (3) low potential for temporary after-image. If the retinal irradiance or subtended angle is sufficiently large, permanent eye damage from retinal burn may occur (e.g., from concentrating mirrors). Below the retinal burn threshold, a region exists where a sufficiently high retinal irradiance may cause a temporary after-image, which is caused by bleaching (over-saturation) of the retinal visual pigments. The size and impact of the after-image in the field of view depends on the size of the subtended source angle. For a given retinal irradiance, smaller source angles yield smaller after-images, and the potential impact is less. Sufficiently low retinal irradiances and/or subtended angles of the glare source have a low potential for after-image and ocular impacts.

A number of factors can affect both intensity and perceived impact of glare: direct normal irradiance (DNI), reflectance, distance, size of the reflecting surfaces, and human factors. DNI is the amount of solar irradiance striking a surface perpendicular to the sun's rays. A typical clear sunny day may yield a DNI of ~1,000 watts per square meter at solar noon, with lower values in the mornings and evenings. DNI provides the starting "strength" of the solar glare source, which can then be reduced by the reflectance of the mirror or receiver. The reflected light can be characterized as a combination of specular (mirror-like) and diffuse (scattered) reflections. Smooth surfaces such as mirrors and smooth glass produce more specular reflections with greater intensity and tighter beams, while rough surfaces produce more diffuse reflections with lower solar intensities but greater subtended angles. In general, specular reflections pose a greater risk for ocular hazards.

The distance between the observer and the glare source can impact both the retinal irradiance and subtended source angle. Atmospheric attenuation caused by particulates or humidity in the air will reduce the retinal irradiance with increasing distance. In addition, for a fixed size of the glare source, larger distances will typically yield smaller subtended angles of the glare source.

Finally, human factors such as ocular properties (pupil size, eye focal length, ocular transmittance) and light sensitivity will affect retinal irradiance, subtended angle and perceived impact of glare. Typical ocular properties for daylight adjusted eyes are provided in Ho, *et al*. [4] and are repeated in the Nomenclature section.

Without atmospheric attenuation, the retinal irradiance [W/m^2] is independent of distance since the power entering the eye (numerator in Eqn. 1) and exposed retinal area (denominator in Eqn. 1) decrease at the same rate with increasing distance. For reflections off a target surface and a given source strength (e.g., sun), the retinal irradiance is given by

$$E_r = \left(\frac{\rho E_{DNI}}{\beta^2}\right)\left(\frac{d_p^2 \tau}{f^2}\right), \qquad (1)$$

where the first group of parameters depends on the source (i.e. target reflectance, source irradiance and source subtended angle), and the second group are the ocular parameters (i.e. pupil diameter, ocular transmittance and focal length). For the analyses provided in this paper, the ocular parameters and DNI are kept constant; values are provided in the Nomenclature. From Ho, *et. al.*, the maximum retinal irradiance that yields an after-image is given by

$$E_{r,flash} = \frac{3.59\times10^{-5}}{\omega^{1.77}}, \qquad (2)$$

which is shown by the green linear curve in Figure 3. The area below this curve (indicated by the light green color) is the preferred zone if in the presence of glare. If the reflections (i.e. glare) from PV modules can be driven below this curve, glare hazards can be minimized.

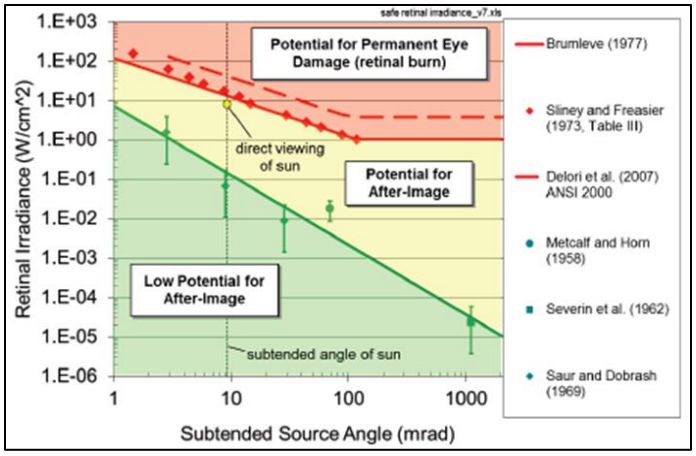

Figure 3. Potential ocular impacts of retinal irradiance as a function of subtended source angle (permission from [[3]]). Note that 1 Watt yields approximately 100 lumens of visible light in the solar spectrum [2].

2.4. Ocular Impacts of PV Surface Texturing

Using Eqns. 1 and 2, a safe retinal irradiance can be determined. That is, for a particular source subtended angle, a retinal irradiance value can be determined that will yield a low potential for an after-image. From Eqns. 1 and 2 a safe retinal irradiance can be satisfied by

$$E_r < E_{r,flash} \,. \tag{3}$$

Inserting all the parameters and solving for the beam spread, β, yields

$$\beta > \left(\frac{\rho E_{DNI} d_p^2 \tau}{f^2 \cdot 3.59\times10^{-5}}\right)^{\frac{1}{0.23}}, \tag{4}$$

which is a function of the reflected source strength (reflectance, ρ, and E_{DNI}). This function is plotted against the surface reflectance as a blue curve in Figure 5, which divides regions of "low-potential" and "potential" for an after-image from glare. A source irradiance of 1,000 W/m^2 is assumed.

3. RESULTS

3.1. Surface Roughness & Reflected Beam Spread

Table 1 provides the measured surface statistics and reflected beam spread from a representative selection of PV module samples. The panels were categorized by surface texturing using the measured RMS surface roughness values: smooth (<1.5 μm RMS), lightly textured (1.5-4 μm RMS), moderately textured (4-10 μm RMS), and deeply textured (>10 μm RMS). The limits of the RMS surface roughness for the categorization were established somewhat arbitrarily; currently there is no known standard for this categorization.

Most of the PV modules exhibited random surface texturing (see contour plots in Figure 7 in the Appendix). That is, the texturing did not show repeating patterns. When performing the Fourier analysis on the surface data, multiple frequency peaks emerged. The first 2-3 peaks typically showed relatively high strengths compared to the subsequent frequency peaks. Therefore, for each PV module the surface spatial period (Λ) was averaged by weighting the first 2-3 period peaks on their relative strength. The deeply textured sample (contour plot shown in Figure 6a in the Appendix) showed periodic surface structure. In this case, a single frequency showed high strength; a weighted-average was not performed in this case.

Table 1. Measured parameters of several representative PV modules (min and max of the S_q values of the PV modules that were measured for the surface texturing categories specified).

Panel Type	S_q (μm RMS)	Λ (mm)	β (mrad)
Smooth Surface 1 (float glass)	0.10	1.28	20
Smooth surface 2	1.49	1.02	137
Lightly textured 1	1.51	0.97	92
Lightly textured 2	2.74	1.09	173
Moderately textured 1	3.80	1.08	175
Moderately textured 2	3.99	1.07	184
Deeply Textured	20.03	0.77	~1,000*

* Roughly estimated since it was not measurable with our instruments (see Figure 2, right image).

3.2. Beam Spread & Surface Roughness Correlation

In Figure 4 a graph of the measured reflected beam spread against the RMS surface roughness scaled by the surface period variations (S_q/Λ) is provided. A power law function of the form $y = Ax^m$ is fitted to the data. Of the PV module samples that we acquired, most of them had light surface texturing. To balance the distribution of the different surface textured samples, more weight was given to samples that were not lightly textured during the data fitting calculation. Otherwise, the fit would be skewed by the lightly textured samples. Due to the increased weighting of some of the data points, the correlation coefficient, R^2, increased.

The data shows a general trend of increasing reflected beam spread (scattering of the reflected glare) with increasing surface roughness-period ratio (S_q/Λ).

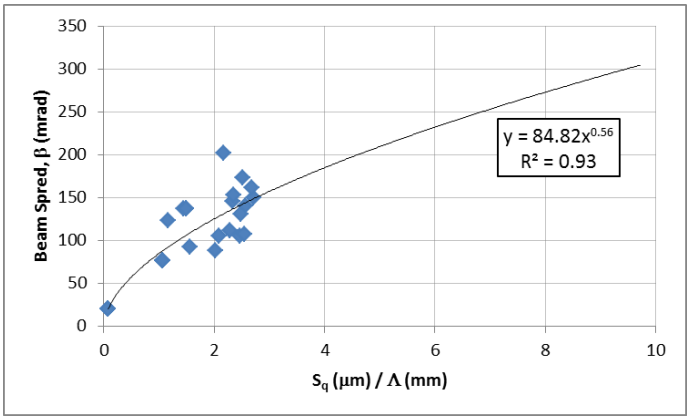

Figure 4. Correlation between the measured solar reflected beam spread and the measured surface roughness. The curve fit follows the power law.

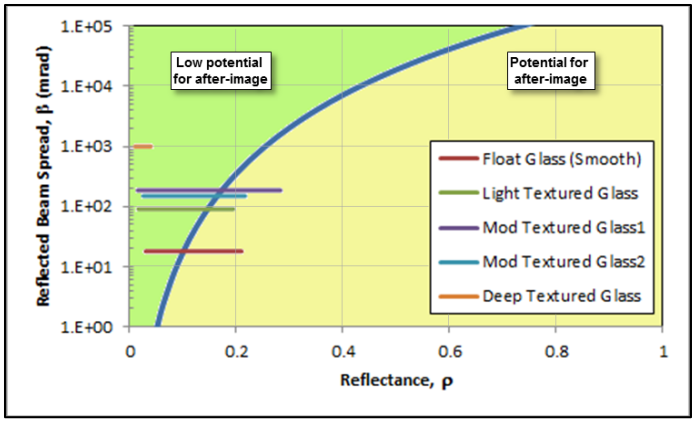

Figure 5. Reflected beam spread versus reflectance to determine potentials for retinal after-image for a representative PV module samples.

3.3. PV modules with Low Glare Hazard Potential

Figure 5 shows a plot of the reflected beam spread (i.e. subtended source angle) versus PV module reflectance. Eqn. 4, plotted as blue curve, provides a boundary for glare after-image from "low potential" to "strong potential", assuming a sun irradiance of 1,000 W/m^2 and using typical values for the ocular parameters. The left side of the curve provides a low potential for glare after-image. The plot shows that as the reflected beam spread (scattering) increases, the reflectance threshold value that yields an after-image increases as well. Therefore, low-reflectance surfaces that yield large scattering are best for reducing the impacts of glare.

Also plotted in Figure 5 are the measured reflected beam spreads versus the measured reflectances (minimum to maximum values over incidence angles they are measured) for representative PV modules. The reflectances were measured over 20-80° angles of incidence in increments of 20° [8]. The β vs. ρ plot for float glass extends over the blue boundary curve suggesting at near normal incidence viewing (ρ ~ 4%) glare impacts are minimal. However, at higher incidence angles, the glare impact potential increases because the reflectance increases with increasing incidence angles.

The data for the lightly textured glass shows mostly low potential for glare impacts until it crosses the boundary for reflectances at high incidence angles, for example when the sun is near the horizon. Similarly, the plots for the moderately textured samples cross the boundary at high solar incidence angles.

The beam spread from the deeply textured samples was roughly estimated since the reflected beam image did not exhibit a clear reflected beam pattern (see PV module sample in Figure 2). The data for the deeply textured sample shows it has very low potential for glare impacts over all incident angles.

4. DISCUSSION

Minimizing glare impacts with smooth float glass at all incidence angles would be difficult. Therefore, the surface should be textured to simultaneously increase diffuse reflections (thus the beam spread) and reduce the reflectance magnitude (see Figure 5) over all solar incidence angles. A deeply textured surface immediately addresses both aspects. A low reflectance at all incidence angles also suggests higher transmittance of the sunlight to the solar cells, assuming no or minimal absorptance by the protective cover material. By conservation of energy, minimizing the reflectance can maximize the transmittance for increased energy production from the solar cells. However, an important aspect of the PV performance is the cleanliness of the PV module surfaces. Soiling of the panels can reduce the performance rapidly. It is not known if deeply textured surfaces would be susceptible to higher soiling rates. This can be addressed in future studies.

Of the PV samples studied, only a few were labeled to have anti-reflection (AR) coatings. These samples exhibited low reflectances at near normal incidence angles, but the coatings did not seem to reduce the reflectance at higher incidence angles – in some cases they showed similar reflectances as the modules without the coatings [8].

4.1. PV surface texturing design considerations

Using a combination of Figures 4 and 5, a design on the surface texturing that minimizes glare impacts may be determined. An upper bound of the module reflectance (corresponding to a large incidence angle) can be first identified, and from Figure 5, the minimum reflected beam spread can be determined that will provide a low potential for after-image for the specified reflectance. For example, a maximum module reflectance of 0.15 would require that the minimum reflected beam spread be greater than ~150 mrad (from Figure 5). The beam spread value can then be used in

Figure 4 to find the necessary surface texturing ratio (S_q/Λ) to achieve the minimum reflected beam spread. In this example, a minimum surface texturing ratio (S_q/Λ) of 2.8 would be required to yield a beam spread of >150 mrad. Although there is a general trend observed in Figure 4, there is variability in the data. Therefore, there is no deterministic beam spread to surface roughness relation. In addition, once a surface texturing ratio is determined, many possible combinations of S_q and Λ exists to achieve the same ratio value. Starting with reasonable values (i.e. values close to those measured in this study) is suggested. A desired surface texturing would be one that results in reflected beam spread and reflectance values to the left of the blue curve in Figure 5.

5. CONCLUSIONS & FUTURE WORK

Twenty-six PV module samples were evaluated for reflectance at various incidence angles, surface roughness, and beam spread upon reflection of the sun (i.e. glare). The results of the reflectance measurements were reported in Yellowhair, *et al.* [8]; parts of the data were used in this paper. In this study, finding correlations between the measured glare from the PV modules and the measured surface roughness ratio (S_q/Λ) were attempted. A plot of the data followed a power law distribution.

From previous studies on solar glare impacts, the retinal irradiance required for low potential for a glare after-image were determined. By re-arranging the parameters, we determined a relation between the beam spread and the PV module reflectance that defines the boundary for glare after-image potential. The measured data were plotted on the same chart (Figure 5) and showed that at high reflectance values (e.g., high incidence angles), there is risk for glare after-image for most of the PV samples tested. However, the deeply textured sample had low reflectance values at all incidence angles and produced a significant amount of scattering and beam spread; therefore, the potential for after-image from this PV module sample was low. The low reflectance of the deeply textured glass also suggests that it yields a high transmittance at all incidence angles, thus allowing more energy production from the solar cells. Its susceptibility to soiling, however, is not known.

For future work, absorptance measurements of PV covers can be performed to get a better assessment of the transmittance magnitude. In addition, soiling studies of glass/polymer samples with different surface roughness will enable a better assessment of surface textures that both mitigate glare while maximizing transmittance to the solar cells.

ACKNOWLEDGEMENTS

The authors thank Evan Bush, a former student intern from the University of Louisville, for assisting in the collection and analysis of the PV glare data. Sandia National Laboratories is a multi-program laboratory managed and operated by Sandia Corporation, a wholly owned subsidiary of Lockheed Martin Corporation, for the U.S. Department of Energy's National Nuclear Security Administration under contract DE-AC04-94AL85000. The United States Government retains and the publisher, by accepting the article for publication, acknowledges that the United States Government retains a non-exclusive, paid-up, irrevocable, world-wide license to publish or reproduce the published form of this manuscript, or allow others to do so, for United States Government purposes.

REFERENCES

[1] Feldman, D., *et al.*, 2012, "PV Pricing Trends: Historical, Recent, and Near-Term Projections," NREL/LBNL Technical Report DOE/GO-102012-3839.

[2] Jakubiec, J.A. and Reinhart, C.F., 2014, "Assessing Disability Glare Potential Due to Reflections from new Constructions: A Case Study Analysis and Recommendations for the Future," in 2014 Transportation Research Board 93rd Annual Meeting, Washington, D.C., January 12-16, 2014.

[3] Ho, C.K., "Relieving a Glaring Problem," in Solar Today 2013, American Solar Energy Society: Boulder, CO. pp. 28-31.

[4] Ho, C. K., Ghanbari, C.M., and Diver, R. B., 2011, "Methodology to Assess Potential Glint and Glare Hazards from Concentrating Solar Power Plants: Analytical Models and Experimental Validation," J. Sol. Engr., 133(3), pp. 1-8.

[5] Fowles, G. R., 1975, Introduction to Modern Optics, 2nd Ed., Dover Publications, Inc., New York, Chap. 2.

[6] Bennett, H. E., and Porteus, J. O., 1961, "Relation between Surface Roughness and Specular Reflectance at Normal Incidence," J. Opt. Soc. Am., 51(2), pp. 123-129.

[7] Vorburger, T. V., and Raja, J., 1990, "Surface Finish Metrology Tutorial," US Dept. Commerce, National Institute of Standards and Technology Report No. NISTIR 89-4088.

[8] Yellowhair, J., and Ho, C. K., 2014, "Reflectance Measurements of Different Glass Surfaces for Photovoltaic Modules," to be submitted for publication.

APPENDIX

6. COMPARISON OF PV MODULE SURFACES

In this section, a few measured PV module surfaces with the optical profilometer are provided for comparison. The measurement area for each sample is about 3 mm × 3 mm.

6.1. Smooth vs. roughly textured surface

Figure 6 shows contour plots of float glass, which has a smooth surface, and the deeply textured surface. The deeply textured surface was deliberately designed by the manufacturer to have a periodic structure in this case. Float glass, as manufactured, typically has a smooth surface finish. Note that the colorbar scale for Figure 6a is one order of magnitude less than 6b since float glass is much smoother than the deeply textured surface.

The float glass is fairly flat and smooth. The reported surface period (Λ) variation of 1.26 mm is mostly noise since the Fourier analysis showed a low signal strength for the period peak.

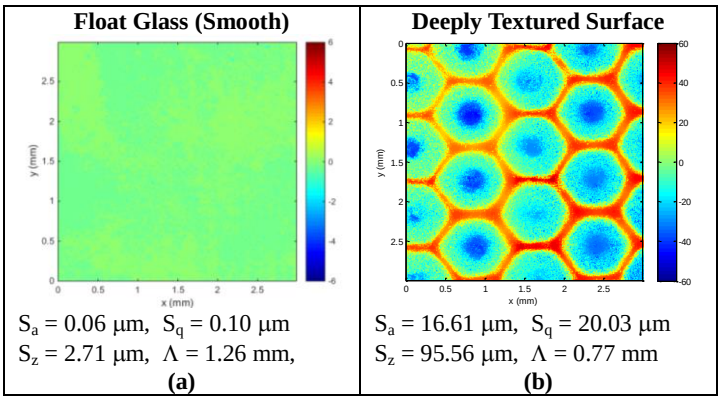

Figure 6. Contour plots of (a) float glass (smooth surface) and (b) a deeply textured surface. The colorbar scale is in microns. Red indicates the highs and blue indicates the valleys in the surface.

6.2. Lightly textured surfaces with varying surface periods

Most of the PV modules studied appeared to have random surface structures as seen in the contour plots in Figure 7, where two lightly textured surfaces are compared. They exhibit similar RMS surface roughness values, but very different surface period variations – the surface period in Figure 7a is about double that of Figure 7b. The effects of the surface period variations on glare were not studied, but could be evaluated in the future.

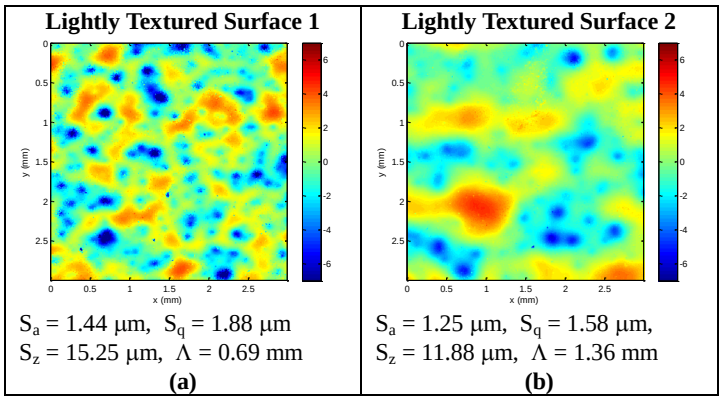

Figure 7. Contour plots of two lightly textured surfaces, but with different surface period variations. The surface in (a) exhibits high period variations, and (b) shows low surface frequencies.

7. PV SURFACE REPLICATION ACCURACY

The surface replication accuracy verification was performed using one of the developmental PV module samples (i.e. a single-cell PV module). This PV module was small enough to fit on the profilometer sample holder. Both the actual PV module (master) and its replica were measured with the optical profilometer at two different locations on the surface and the measurements were averaged. Note that the same points on the master and replica were not measured; finding the identical points (over a 3×3 mm^2 area) on the master and replica would be have difficult and time consuming. Figure 8 shows one of the measurements on the master and its replica. Table 2 summarizes the measured surface statistics.

Table 2. Measured surface roughness of the master sample and its replica to assess the replication accuracy.

	Master Avg. Measurement	Replica Avg. Measurement	% Error
AVG Surface Roughness, S_a (μm)	1.85 ± 0.18	2.00 ± 0.05	7.7
RMS Surface Roughness, S_q (μm RMS)	2.45 ± 0.24	2.61 ± 0.13	6.6

The RMS surface roughness agreed to within 7% between the replica and the actual surface. The replicas generally had higher RMS surface roughness values. This could be due to form errors that remained in the surface measurements. Although the rubber-like replicas were thick (3-4 mm), they were still able to bend and flex slightly. In addition, the

measured replica surfaces were more "grainy" as seen in the contour plots in Figure 8.

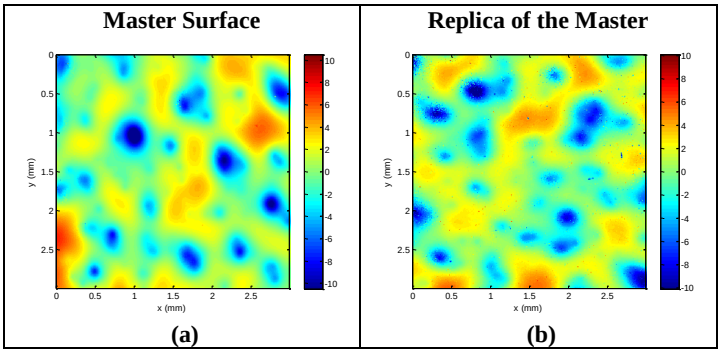

Figure 8. Contour plots of a (a) master surface and (b) replicated surface of the master. Note that these are not the same points on the master and replica; locating the same points (over 3×3 mm^2 area) would have been difficult and time consuming.